Nano-Scale Porosity Analysis of a Permian Tight Gas Reservoir*

Philipp Antrett[1], Alexandra Vackiner[1], Uwe Wollenberg[1], Guillaume Desbois[2], Peter Kukla[1], Janos Urai[2], Harald Stollhofen[3], and Christoph Hilgers[4]

Search and Discovery Article #40821 (2011)
Posted October 17, 2011

*Adapted from expanded abstract presentation at AAPG International Conference and Exhibition, Milan, Italy, October 23-26, 2011.

[1]Geological Institute, RWTH Aachen University, Germany (antrett@geol.rwth-aachen.de)
[2]Geologie/Endogene Dynamik, RWTH Aachen University, Germany
[3]North Bavarian Center of Earth Sciences, FAU Erlangen-Nuernberg, Germany
[4]Reservoir Petrology, RWTH Aachen University, Germany

Abstract

We present the first results of a high resolution petrographic study as part of a multidisciplinary research project focusing on the evolution of Permian tight gas reservoirs in the Southern Permian Basin in Northern Germany. The SEM-BIB (scanning electron microscopy – broad ion beam) technique enables pore visualisation on polished surfaces down to nm-scale. The ion beam preparation thus provides unprecedented insights into pore geometries and morphologies of low porous rocks in general. In the first phase of this project, selected pores of Rotliegend tight gas samples were investigated. Initially, different phases of clay mineral growth (illite and chlorite) could be identified and the relative timing of crystallization was established. The focus lay on the analysis of clay mineral coatings of quartz grains. These play a major role during diagenesis, inhibiting porosity and permeability reduction through quartz overgrowth or pressure solution. Observations further revealed that chlorite crystallization may prevent the growth of illite which restricts porosity and permeability reduction by secondary illite to areas where chlorite is the dominant pore cementing phase. Results supported and refined our detailed sedimentary facies analysis from core material of the Upper Rotliegend II in aeolian reservoirs. In addition, possible stress indicators were also identified, which might provide crucial information for future field development. Future work will include a geometrical 3D analysis of selected samples and investigations of grain coatings in modern dune fields.

Introduction

With growing energy needs and further exploitation of conventional hydrocarbon reservoirs the importance of tight gas reservoirs has increased dramatically during the last years. However, porosity and permeability reducing processes in these reservoirs often remain

enigmatic. Studies concerning seismic interpretation, seismic attribute analysis and well log information often reach a dead-end when closely spaced changes in the depositional and structural environments occur.
In this study we investigate a new approach of qualitative and quantitative reservoir petrology on samples from a tight gas field in the Upper Rotliegend II (Upper Permian) in Northern Germany. In a marginal position to the great Rotliegend playa lake in the Southern Permian Basin (Fig. 1), reservoir rocks of fluvio-aeolian origin were deposited under arid climate. During diagenesis, rocks have undergone an increased degradation of porosity and permeability triggered by migrating fluids (Gaupp and Solms, 1993; Gaupp 2005). Enhanced cementation such as an increased quartz overgrowth and secondary clay mineral crystallization were the results of this porosity inverting processes, which were mainly recognized in aeolian (dune) deposits. The timing of this diagenetic effect and its relation to stress induced fluid pathways such as fractures and faults are not fully understood.

We apply scanning electron microscopy – broad ion beam (SEM-BIB) analysis (Desbois, 2011) and thin section analysis for diagenetic observations, the quantification of pore symmetries and porosity estimation. Porosity and mineral content of a sample is analysed by image analysis software. The new technique overcomes the low resolution of standard optical microscopy when porosity and pore symmetries cannot be quantified in areas where clay is the dominating mineral e.g. clay replacing feldspar mineral grains. To visualize and quantify porosity distribution and symmetry in such areas we analyse SEM-BIB images with the focus on inter-clay porosity. We upscale the SEM-BIB results, calculating porosity values and clay volumes derived from blue stained thin sections. Information about pore shapes and volumes can be used as input for fluid flow modelling. The aim of this study is to develop an automated workflow that provides reproducible results.

Geologic and Sedimentary Setting

The W-E trending Southern Permian Basin (SPB) extends from the UK across the southern North Sea, covering northern Germany, Poland and the Baltic States, varying in width between 300 and 600 km. The basin centre was situated in Northern Germany. It reached its maximum extension during the Late Upper Rotliegend II, covering an area of ~429,000 km. The tight gas field investigated is located in Upper Rotliegend II in the southwestern part of the SPB in NW-Germany (Figure 1). During the arid to semi-arid climate, sedimentation was dominated by siliciclastics and only minor evaporites (Glennie, 1972). Four major facies associations were identified by George and Berry (1993), Strömbäck and Howell (2002) and Legler (2005): ephemeral fluvial (wadi), aeolian, sabkha and lacustrine environments. Strong aeolian winds supplied a huge amount of aeolian sediment from the east (Glennie, 1983a, Gast et al., 1998 and Rieke, 2001). In addition, sediment was provided by ephemeral fluvial systems sourced by the Variscan Orogen and local highs in the south. Sedimentary facies analysis by Vackiner et al. (2010) on cores of the investigated tight gas field reveals a close interbedding of dry aeolian sediments (dune, dune base and dry sandflats) with low clay contents with wet aeolian, interdune and lake/pond deposits (damp and wet sandflats and mudflats) with higher clay contents. The maximum dune interval in the cores is ~2.5 m.

Data and Methods

Our analysis is based on core material of 2 wells. In addition to optical microscopic analysis of blue stained thin sections, SEM-BIB samples with a very smooth surface were produced using a stand-alone argon ion beam cross section polisher (JEOL SM-09010, Erdmann et al., 2006) and a Zeiss Supra 55 electron microscope equipped with an EDX detector (EDAX, Apollo 10; Desbois et al., 2011). Images were taken at a magnification of 3000X. SEM imaging studies were performed at 15 kV at a working distance of 10 mm to guarantee the consistent contrast that is required for the image stitching process and the threshold adjustment during image analysis. Thin sections were digitalized at 25 times magnification using the Leica DM 4500 P polarisation microscope equipped with a Leica DFC 295 camera and a PC workstation with the IQ-WinLight software package. Panoramic images of thin sections and SEM-BIB were compiled/stitched using the Autopano Giga 2.5 software by Kolor (www.kolor.com). Optical microscopic images consisted of ~80-100 individual images, SEM-BIB panoramic images of ~340-400 individual images. The stitched images enable a continuous, dynamic zoom from the polished surface of 1.5 mm² down to pores of mm² size. For pore shape/symmetry and porosity analysis the open source software JMicroVision V.1.25 (Roduit, 2011) was used. In blue stained thin sections porosity and clay content were determined by adjusting a threshold manually. We used SEM-BIB images, backscatter electron microscope (BSE) images and EDX measurements for mineral identification. In a first step, clay minerals are identified and then isolated using standard image editing software. By manually adjusting a threshold in JMicroVision the inter-clay porosity was determined (Figure 2). The total porosity of the sample was calculated by adding the porosity determined from the blue stained pores in the thin section to the inter-clay porosity from the SEM-BIB image (Figure 3). The inter-clay porosity was calculated from the percentage of inter-clay porosity from the SEM-BIB image and the clay content of the thin section:

$$\Phi_{tot} = \Phi_{ts} + ICP \bullet CM_{ts}$$

Φ_{tot} = total porosity; Φ_{ts} = porosity in blue stained thin section; ICP= inter-clay porosity;

CM= clay mineral content in thin section

A minimum threshold of 10 pixel^2 (equals an area of 0.7 mm^2 in the thin section and 0.096 mm^2 in the SEM BIB image) was established to eliminate pixel errors and to avoid false pore statistics.

Results of porosity analysis were compared to porosities derived from sonic velocities. In pore symmetry analysis, the pore area (2D) and the elongation (long axis vs. short axis) were determined. All the results directly provide the input information for fluid flow modelling.

Results

Diagenetic Observations, Pore Symmetry Quantification and Upscaling Approach

The SEM-BIB technique enables pore visualisation down to nm scale. The argon ion beam preparation enables unique insight into pore geometries and morphologies (Desbois, 2011). The number of individual pores per sample in the so far investigated 7 SEM-BIB images

varies between ~20.000 and ~80.000. With the information provided by EDX and SEM-BIB analysis a relative timing of crystallization was established (Figure 4) and compared to existing analysis of diagenetic evolution of the Permian tight gas reservoir by Havenith et al. (2010). Especially with regard to different generations of clay mineral growth these well polished samples provided valuable additional information.

Aeolian deposits show non-continuous illite and chlorite coatings around detrital quartz and feldspar grains (Figure 5). Information about the timing of hydrocarbon migration was derived from euhedral titanite, growing on multiple generations of clay minerals (Figure 5). In addition stress indicators were identified. Coarse chlorite meshwork in the pore space blocks/inhibits later illite growth and thus passively preserves initial porosity (Figure 6).

In this study, we analysed an aeolian dune sample. Pore area quantification of the SEM-BIB image shows that the pore fraction with the smallest pore area with a pore size between 0.0961 mm2 and 1 mm is most abundant (82%, Figure 2). However, they only cover a relatively small area of 22%. Pore symmetry was determined by the elongation and the ratio of long and short pore axis with a dominant elongation between 0.25 and 0.49 (Figure 2).

In a second sample, an upscaling approach was applied combining information from thin sections and SEM-BIB. Colour threshold adjustment in the blue stained thin section gave a result of 0.9% porosity and an amount of clay minerals including inter-clay porosity of 41.1%. Inter-clay porosity is not further quantifiable with the limited magnification of optical microscopy. Inter-clay porosity in the SEM-BIB sample was 13.6%, which taken into account the inter-clay porosity of 41.1% in thin section, sums up to a total amount of porosity is 6.5%.

Error Calculation

With the intention to quantify the error of manual threshold analysis on SEM-BIB images, three images were chosen in which all the pores were interpreted manually and results compared to the thresholding method. The first sample shows the challenges of this method applied on the 2D images. The SEM-BIB images provide a uniquely long depth of view into the pore that is partly filled by secondary quartz cement, which will also be identified by the threshold (Figure 7). However, the upscaling from 2D sections in 3D only holds true if the pore area estimated from 2D sections is truly 2D. In general, the pore areas identified by automated interpretation are always underestimated (Fens, 2010). We thus manually tracked pores, which gave a result of 11.5 ± 0.6%, while threshold analysis is estimated 10.4 ± 0.1% porosity for an individual image (Figure 7). Whereas the estimated porosity by calculation will be lower in an automated analysis, the induced fractures within SEM-BIB samples due to releasing stress from well recovery will increase the porosity by 0.6% on the example of image 1 (Figure 7). In two additional images manual interpretation vs. threshold adjustment resulted in: 6.89% vs. 6.08% and 5.21% vs. 4.47%.

For the upscaling from SEM-BIB images to thin sections only the inter-clay pores are of interest, because pores of bigger sizes are quantifiable with thin section analysis. In addition, the 3D effect that is a challenge in the SEM-BIB images is absent in thin sections. Consequently, the major pore shown in image 1, which is not an inter-clay pore, is not included in SEM-BIB analysis. When the fractures

are subtracted from the result of automated analysis the resulting porosity is 9.8%. In comparison, the calculated porosity from sonic velocities is 9.4% ± 1.9 %.

Discussion and Conclusions

The information provided by the SEM-BIB method in addition to optical microscopy improves the diagenetic analysis. The nicely polished samples are a valuable source of additional information, especially concerning the differentiation of multiple clay mineral generations (Figure 5). One example is the observation of non-continuous clay coats around detrital mineral grains, are characteristic for active depositional settings (Esch et al., 2008 and Adjukiewicz et al., 2010). In such systems dunes are restricted in height as a result of high wind velocities and limited sediment supply (Fryberger, 1979). Additionally, abraded clay coats indicate a further sediment transport (Esch et al., 2008 and Adjukiewicz et al., 2010). This observation supported previous core interpretations by Vackiner et al. (2010) and is important concerning the identification of modern reservoir analogues.

Pores can be quantified with respect to their size, distribution, surface, roughness and mineralogical phases in tight reservoirs rocks. Those parameters serve as direct input for fluid flow modelling. Our observations show that uncertainty decreases with increasing areas analysed. In this study a minimum pore value/area was established for pore size interpretation to avoid false statistics and pixel errors. However, the charts (Figure 2) induce that the porosity in even smaller pores which are not considered in this study might only have a marginal influence on poro/perm characteristics. To investigate this assumption, fractal dimensions of pore size distributions as discussed by Krohn and Thompson (1986) and Schlueter et al. (1997) will be investigated in future studies.

The approach of upscaling from SEM-BIB to thin sections improves optical porosity estimation. Further upscaling to core and reservoir scale is investigated in the ongoing study. The application of the technique and the methodology introduced on the example of the tight gas field in Northern Germany can provide improved knowledge and understanding of the reservoir petrology in hydrocarbon reservoirs worldwide.

References

Adjukiewicz, J.M., P.H. Nicholson, and W.L. Esch, 2010, Prediction of deep reservoir quality using early diagenetic process models in the Jurassic Norphlet Formation, Gulf of Mexico: AAPG Bulletin v. 94/8, p. 1189-1227.

Desbois, G., J.L. Urai, P.A. Kukla, J. Konstanty, and C. Baerle, *in press*, High-resolution 3D fabric and porosity model in a tight gas sandstone reservoir: A new approach to investigate microstructures from mm- to nm-scale combining argon beam cross-sectioning and SEM imaging: Journal of Petroleum Science and Engineering, doi:10.1016/j.petrol.2011.06.004

Esch, W.L., J.M. Adjukiewicz, and A.C. Reynolds, 2008, Early Grain-Coat Formation in Chaco Dune Field, New Mexico: Insight into Formation Mechanisms, Distribution, and Implications for Predictive Modeling to Assist in Deep Play Identification: Search and Discovery Article #50135, http://www.searchanddiscovery.com/documents/2008/08201esch/ndx_esch.pdf , Web accessed October 7, 2011.

Fens, T.W., 2000, Petrophysical Properties from small rock samples using image analysis techniques: Ph.D. thesis, Delft University of Technology (Technische Universiteit Delft), Delft, The Netherlands, 199 p.

Fryberger, S.G., and G. Dean, 1979, Dune forms and wind regime, *in* E.D. McKee (Ed.), A study of global sand seas: University Press of the Pacific, p. 137-169.

Gast, R., M. Pasternak, J. Piske, and H.J. Rasch, 1998, Das Rotliegend im nordostdeutschen Raum: Regionale Übersicht, Stratigraphie, Fazies und Diagenese: Geologisches Jahrbuch A, 149, p. 59-79.

Gaupp, R., A. Matter, J. Platt, K. Ramseyer, and J.P. Walzebuck, 1993, Diagenesis and fluid evolution in deeply buried Permian (Rotliegende) gas reservoirs, Northwest Germany: AAPG. Bulletin, v. 77/7, p. 1111-1128.

Gaupp, R., and M. Solms, 2005, Sedimentological and Petrological Investigations, *in* Paleo Oil- and Gasfields in the Rotliegend of the North German Basin: Effects upon Hydrocarbon Reservoir Quality (Paläo-Öl-und Gasfelder im Rotliegenden des Norddeutschen Beckens: Wirkungen der KW-Migration auf die Speicherqualitäts-Entwicklung): DGMK Research Report 593-8: Tight Gas Reservoirs – Natural Gas for the Future, p. 1-1 - 1-44.

George, G.T., and J.K. Berry, 1993, A new palaeogeographic and depositional model for the Upper Rotliegend of the UK Sector of the Southern North Sea, *in* C.P. North and D.J. Prosser (eds.), Characterization of Fluvial and Aeolian Reservoirs: Geological Society, London, Special Publications, v. 73, p. 291-319.

Glennie, K.W., 1972, Permian Rotliegendes of Northwest Europe Interpreted in Light of Modern Desert Sedimentation Studies: AAPG Bulletin, v. 56/6, p. 1048-1071.

Glennie, K.W., 1983a, Early Permian (Rotliegendes) palaeowinds of the North Sea: Sedimentary Geology, v. 34, p. 245-265.

Havenith V.M.J., F.M. Meyer, and S. Sindern, 2010, Diagenetic Evolution of a Tight Gas Field in NW Germany: German Society for Petroleum and Coal Science and Technology (DGMK) Spring Conference (DGMK/ÖGEW Frühjahrstagung), 12-13 April 2010 in Celle, Germany, p. 469-474.

Krohn, C.E., and A.H. Thompson, 1986, Fractal sandstone pores: Automated measurements using scanning-electron-microscope images: Physical Review B, v. 33/9, p. 6366-6374.

Legler, B., 2005, Faziesentwicklung im Südlichen Permbecken in Abhängigkeit von Tektonik, eustatischen Meeresspiegelschwankungen des Proto-Atlantiks und Klimavariabilität (Oberrotliegend, Nordwesteuropa): Schriftenreihe der Deutschen Gesellschaft für Geowissenschaften, Heft 47, 291 p.

Rieke, H., 2001, Sedimentologie, Faziesarchitektur und Faziesentwicklung des kontinentalen Rotliegenden im Nordostdeutschen Becken (NEDB): Ph.D. thesis, Potsdam University, Germany, online resource.

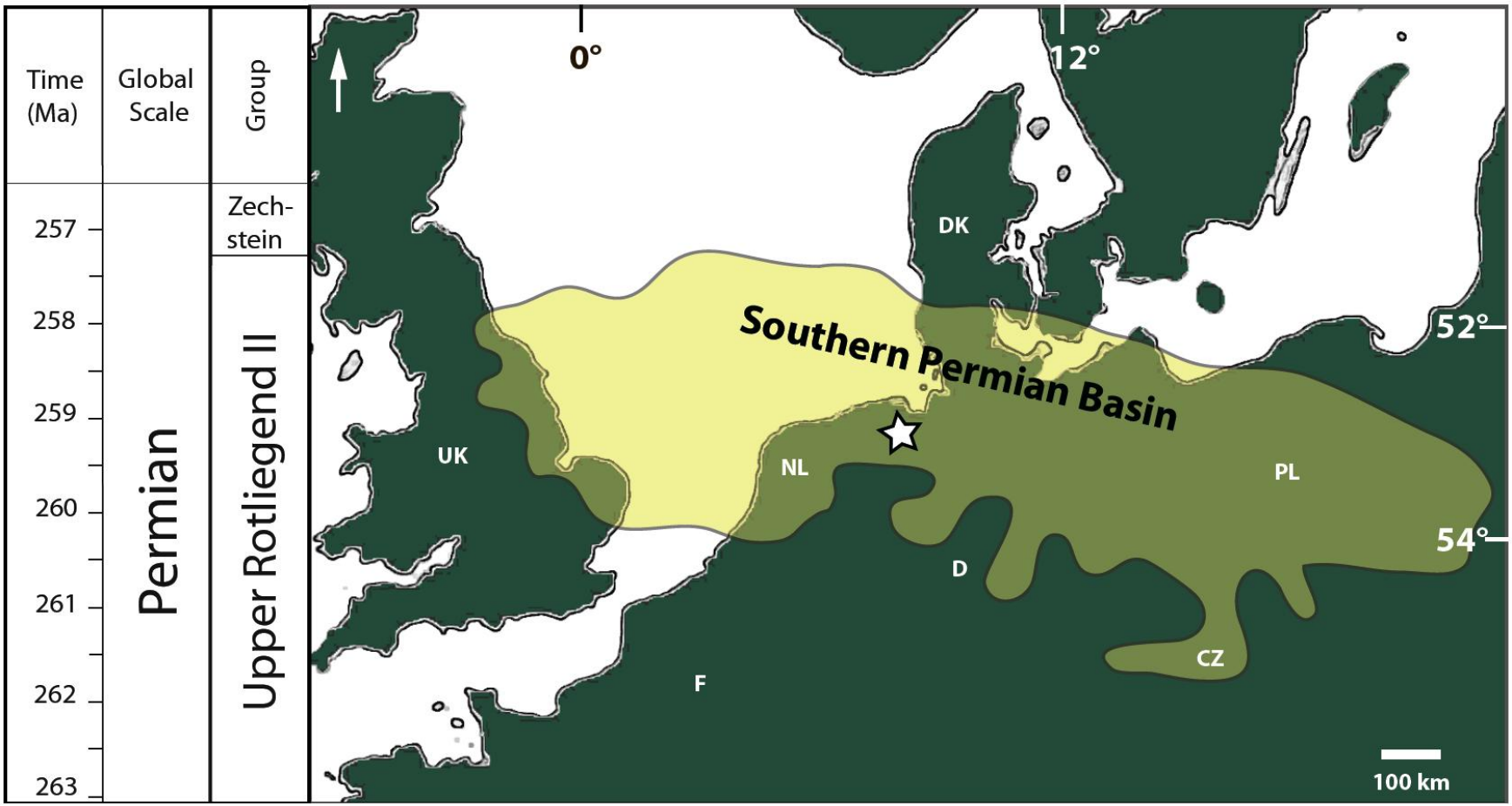

Figure 1. Stratigraphic chart on the left. Maximum extension of the Southern Permian Basin (modified after Ziegler, 1982). Study area marked by the star.

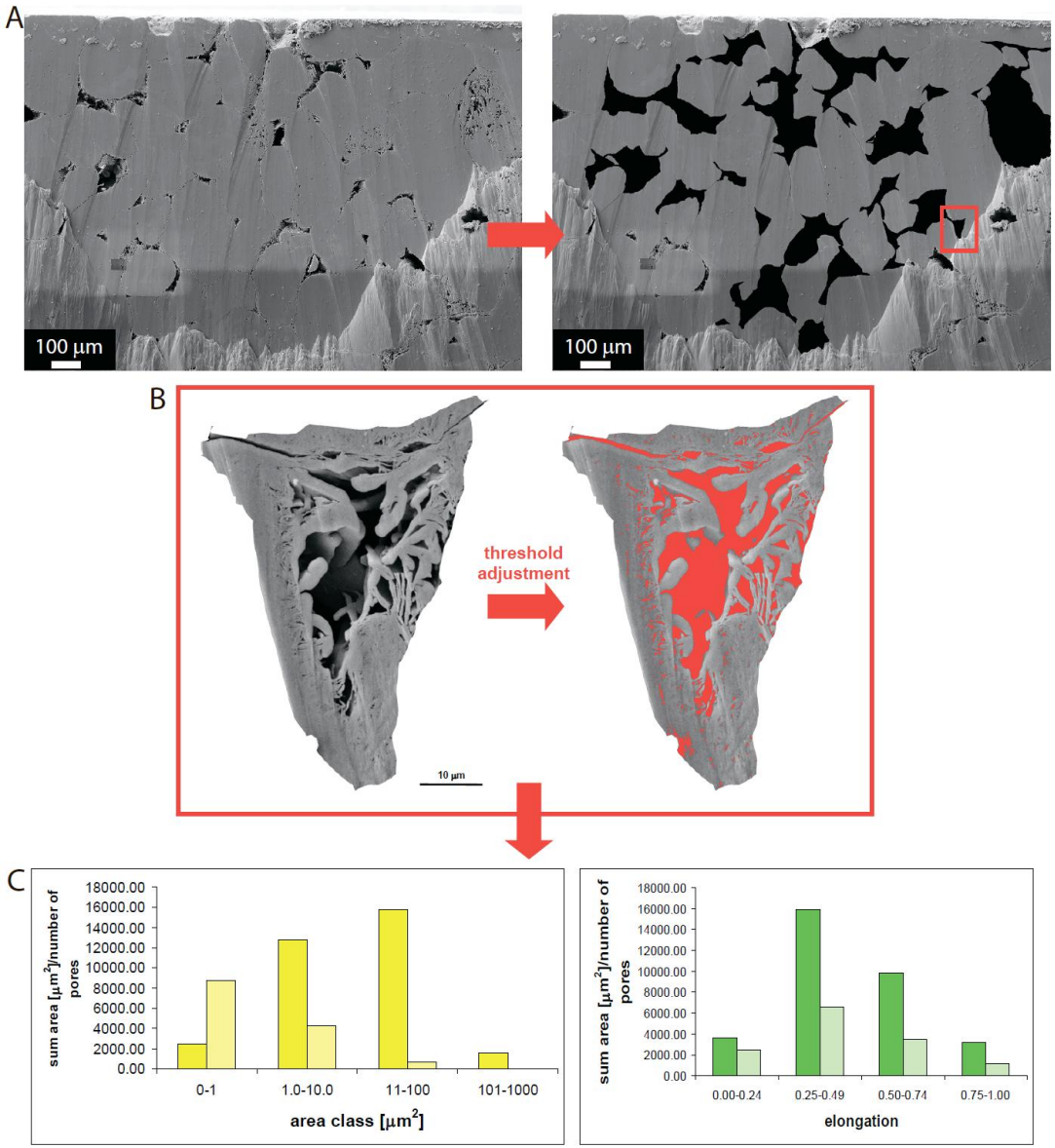

Figure 2. Workflow for inter-clay porosity analysis. A) Identification and isolation of clay minerals. B) Threshold adjustment to quantify inter-clay porosity. C) Results of the pore analysis of the entire sample.

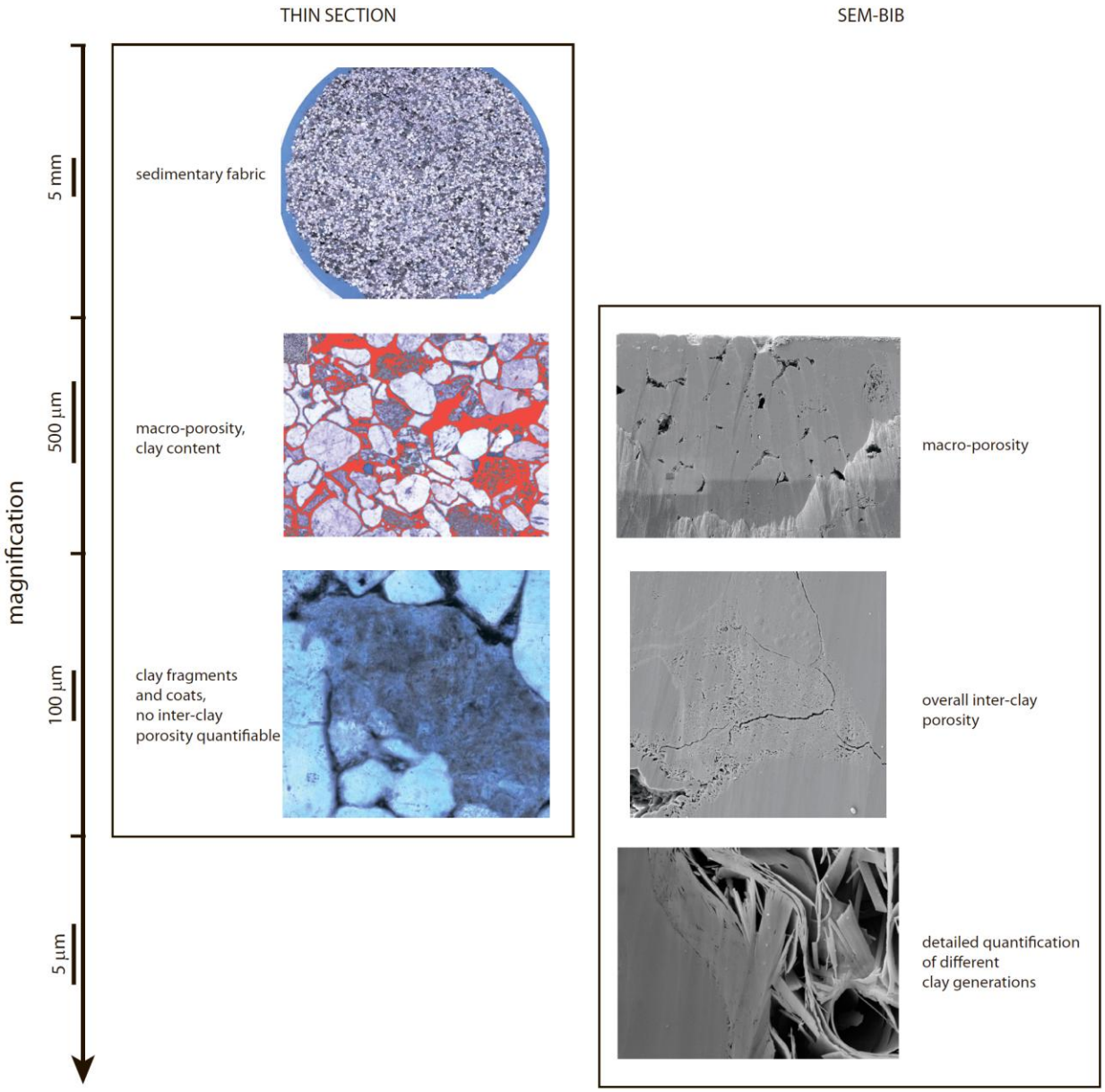

Figure 3. Information available from thin sections and SEM-BIB images at different scales.

Figure 4. Relative timing of crystallization. Comparison of results of optical microscopy (green) and SEM-BIB (blue). Uncertainty displayed in light colours.

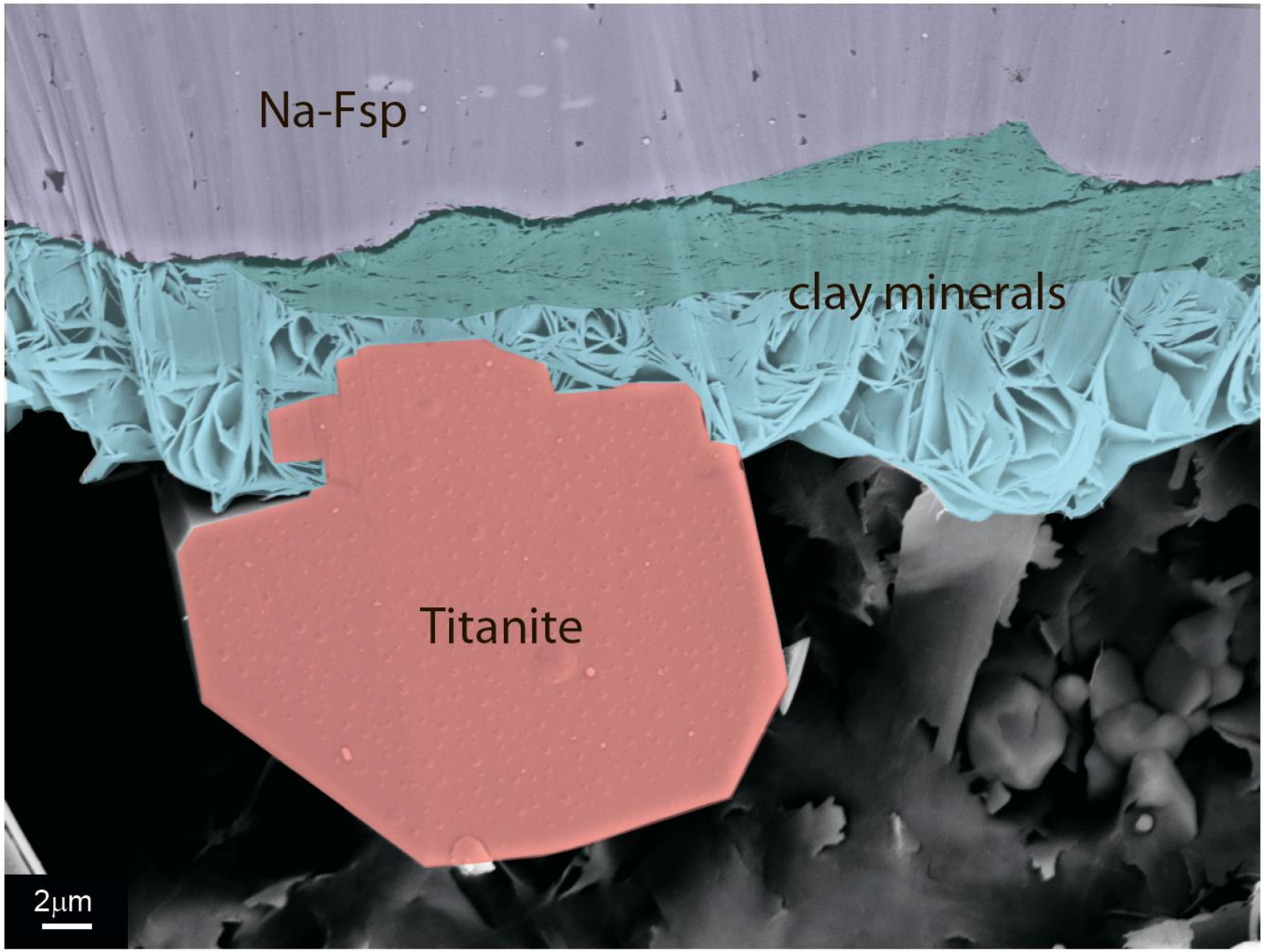

Figure 5. Non-continuous clay coating of a detrital feldspar grain in dark green. The growth of euhedral titanite on two generations of clay minerals is associated with hydrocarbon migration.

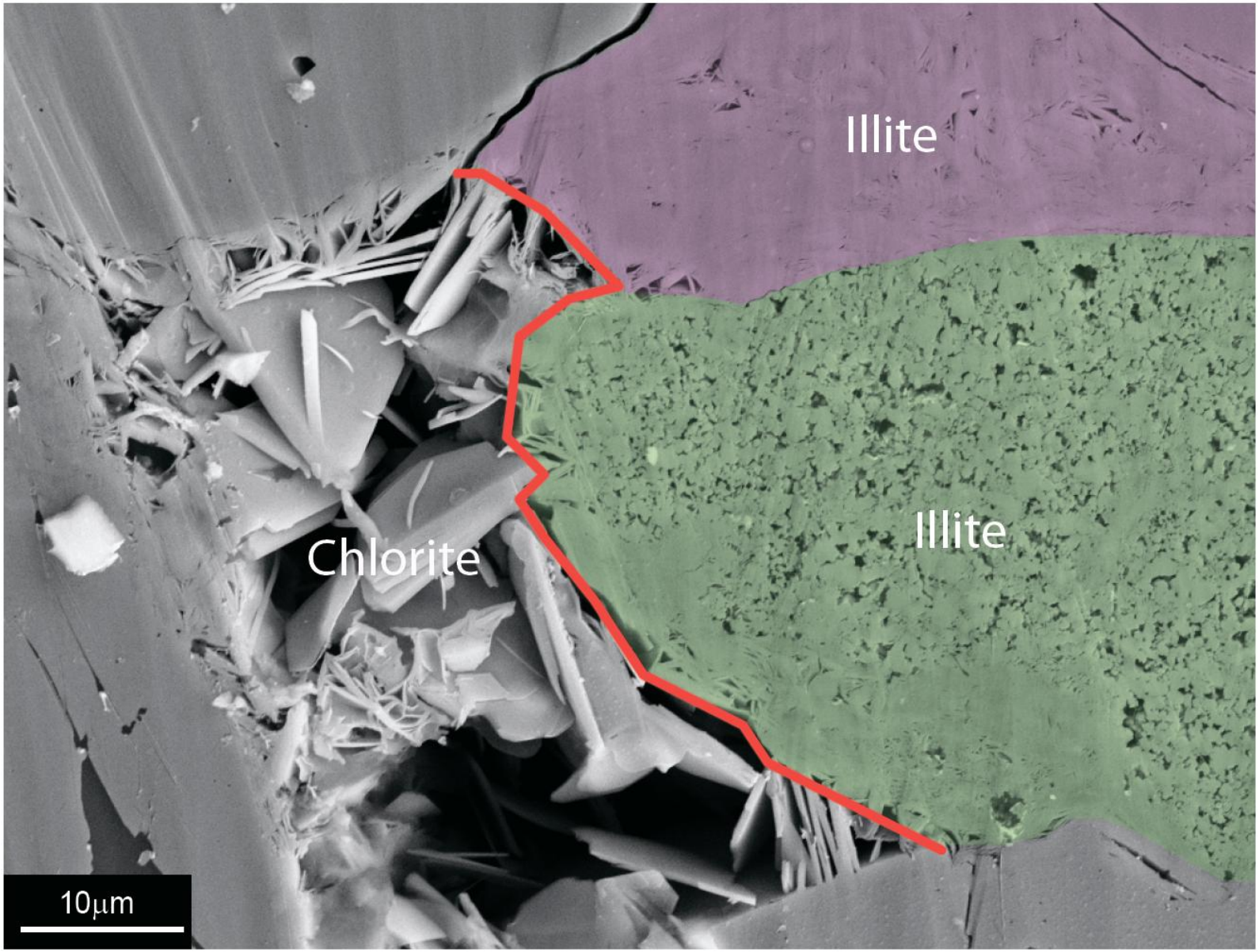

Figure 6. Two generations of illite. Further growth is blocked/inhibited by coarse chlorite meshwork.

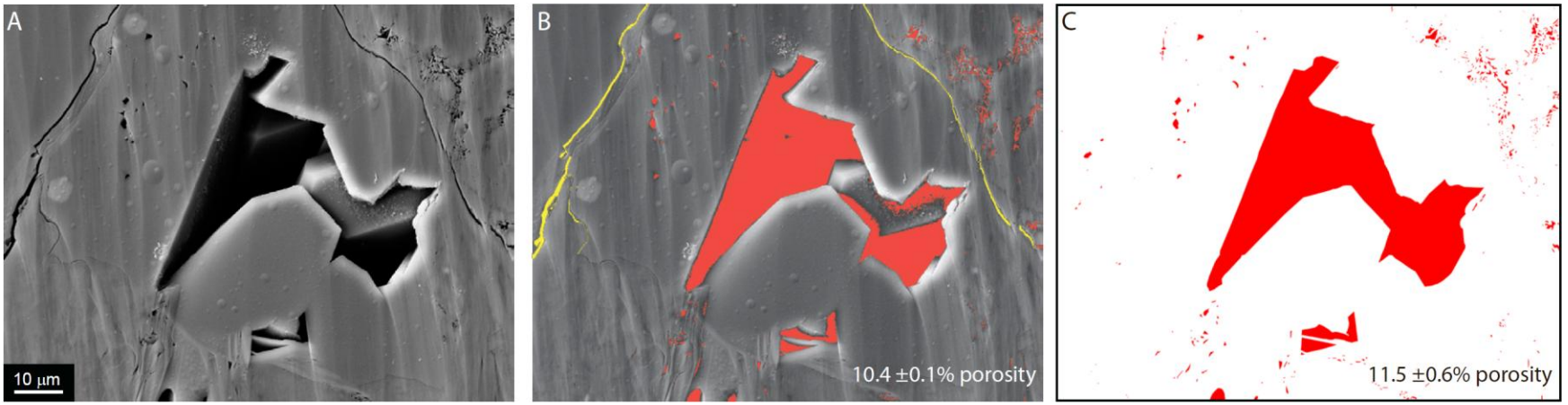

Figure 7. A) Original SEM-BIB image. B) Result of manual threshold adjustment. Euhedral quartz in the pore is a challenge for threshold adjustment. Fractures highlighted in yellow. C) Manual interpretation of porosity.